Molecular Dynamics Simulations of Sorption of Organic Compounds at the Clay Mineral / Aqueous Solution Interface*

BRIAN J. TEPPEN,[1] CHING-HSING YU,[2] DAVID M. MILLER,[2] LOTHAR SCHÄFER[2]

[1]*Advanced Analytical Center for Environmental Sciences, Savannah River Ecology Laboratory, Aiken, South Carolina 29802*

[2]*Departments of Agronomy and Chemistry, University of Arkansas, Fayetteville, Arkansas 72701*

Received 4 June 1997; accepted 10 July 1997

ABSTRACT: The adsorption of trichloroethene, C_2HCl_3, on clay mineral surfaces in the presence of water has been modeled as an example describing a general program that uses molecular dynamics simulations to study the sorption of organic materials at the clay mineral/aqueous solution interface. Surfaces of the clay minerals kaolinite and pyrophyllite were hydrated at different water levels corresponding to partial and complete monolayers of water. In agreement with experimental trends, water was found to outcompete C_2HCl_3 for clay surface sites. The simulations suggest that at least three distinct mechanisms coexist for C_2HCl_3 on clay minerals in the environment. The most stable interaction of C_2HCl_3 with clay surfaces is by full molecular contact, coplanar with the basal surface. This kind of interaction is suppressed by increasing water loads. A second less stable and more reversible interaction involves adsorption through single-atom contact between one Cl atom and the surface. In a third mechanism, adsorbed C_2HCl_3 never contacts the clay directly but sorbs onto the first water layer. To test the efficacy of existing force field parameters of organic compounds in solid state simulations, molecular dynamics simulations of several

*Paper presented in honor of Professor N. L. Allinger.

Correspondence to: B. J. Teppen; e-mail: teppen@srel.edu

Contract/grant sponsor: U.S. Department of Agriculture; contract/grant number: 95-37107-1915 and 97-35107-4362

Contract/grant sponsor: University of Georgia/U.S. Department of Energy; contract/grant number: DE-FC09-96SR18546

CCC 0192-8651 / 98 / 020144-10

representative organic crystals were also performed and compared with the experimental crystal structures. These investigations show that, in general, in condensed-phase studies, parameter evaluations are realistic only when thermal motion effects are included in the simulations. For chlorohydrocarbons in particular, further explorations are needed of atomic point charge assignments.
 J Comput Chem **19**: 144–153, 1998

Keywords: molecular dynamics simulations; clay mineral adsorption; clay mineral parameter development; trichloroethene adsorption on clay minerals; organic chlorine electrostatic charges

Introduction

Chlorinated hydrocarbons dominate lists of the ten most commonly detected organic contaminants in groundwaters of the United States and Western Europe.[1] Among them, trichloroethene (C_2HCl_3) has perhaps the greatest potential to spread[2] from waste-disposal sites to drinking water sources because of its relatively high water solubility, high vapor pressure, and long persistence in subsurface environments. Toxicological concerns have resulted in regulations[3] placing an upper limit of 0.005 mg/L for concentrations of C_2HCl_3 in drinking water in the U.S. The water solubility of C_2HCl_3 is 1385 mg/L,[4] which is more than five orders of magnitude greater than the drinking water limit. Thus, a concerted effort to characterize, understand, contain, and remediate waste plumes of chlorinated hydrocarbons is needed before the plumes further contaminate major aquifers.

From 10 to 10^4 mg/kg C_2HCl_3 sorbs to low-organic-matter minerals,[5–7] so all contaminated aquifer materials are potential long-term sinks and longer-term sources of C_2HCl_3, but little or nothing is known about the mechanisms of adsorption. Clay minerals often comprise the bulk of the surface area in low-organic-matter aquifer materials, so the interactions of C_2HCl_3 and clays are of special interest.

Very few previous simulations[8–12] have studied clay interactions with organic adsorbates and none of these have considered: (a) dynamic motion of either the clay or the adsorbate; or (b) competition with water, which is ubiquitous on natural mineral surfaces. We have recently developed methods for dynamic simulations of clays.[13] Although initial molecular dynamics simulations of organic cation adsorption to clays[13] were able to reproduce experimental data, further testing is necessary to establish that such a force field for clays can be used in conjunction with other, independently derived force fields for water and organic molecules.

The objective of the present study was to explore the behavior of C_2HCl_3 on hydrated clay surfaces. At the same time, we examined a set of commercially available force field parameters and tested their suitability for studying adsorption in concert with our newly created force field for clays.

Methods

All simulations involving clay minerals used our force field created and validated expressly for clays.[13] Parameters for organics and water were taken from the pcff force field distributed by MSI[14,15] and are shown in Table I. The only exceptions were the charges on C_2HCl_3 atoms. To check the charges that pcff assigned to C_2HCl_3, we performed an MP2/6-311 + G(2d, p) geometry optimization followed by a CHELPG analysis,[16–18] which finds partial atomic charges that reproduce the *ab initio* molecular electrostatic potential. The resultant charges, shown in Figure 1, were used to create the bond increments for C_2HCl_3 given in Table I. The simulations reported here used the Discover module of the Biosym molecular modeling suite,[14,15] employed three-dimensionally periodic boundary conditions, and imposed no space group symmetry other than Pl. The molecular dynamics timestep was 0.5 fs, except for simulations of neat CCl_4 and C_2Cl_6, for which the timestep was 1.0 fs. The temperature was controlled by direct velocity scaling and, where applicable, the pressure was controlled by the Parrinello–Rahman method.[15]

We used Karasawa and Goddard's[19] Ewald-inspired lattice sums, as implemented in the Discover code, for calculating both the Coulombic and dispersive contributions to the energies and forces. In this scheme, the Ewald parameter is automati-

TABLE I.
Nonbonded Parameters Used for Water and Organic Molecules in These Studies[a] (All Parameters Except Charges for TCE Were Taken from pcff).[14,15]

Nonbounded (1, 2- and 1, 3-interactions excluded) $E_{ij} = \sum_{i \neq j} \frac{A_i A_j}{r_{ij}^9} - \frac{B_i B_j}{r_{ij}^6} + \frac{332.07 q_i q_j}{r_{ij}}$

Atom type	Description	$[((\text{kcal/mol}) \cdot \text{Å}^9)^{1/2}]$	$([(\text{kcal/mol}) \cdot \text{Å}^6]^{1/2})$
o*	O atom in water	238.3	42.6
hw	H atom in water	0.24	0.26
hc	Generic organic H atom	27.8	6.58
c=	sp2 C atom in TCE	163.5	26.0
cp	C atom in benzene ring	185.2	28.3
c	Generic sp3 C atom	170.2	26.0
cl	Organic Cl atom	313.4	49.5

Charge q_i on an atom is the sum of bond increments δ_{ij} over all bonded neighbors

i	j	δ_{ij}	δ_{ji}
o*	hw	−0.399	0.399
c=	hc	−0.133	0.133
cp	hc	−0.127	0.127
c	hc	−0.053	0.053
c	cl	0.184	−0.184
c=	cl	0.050	−0.050

[a]For the simulations reported in this study, all internal degrees of freedom were allowed to vary. Only the nonbonded terms are tabulated because they govern interactions with the clay and among the molecules in a crystal.

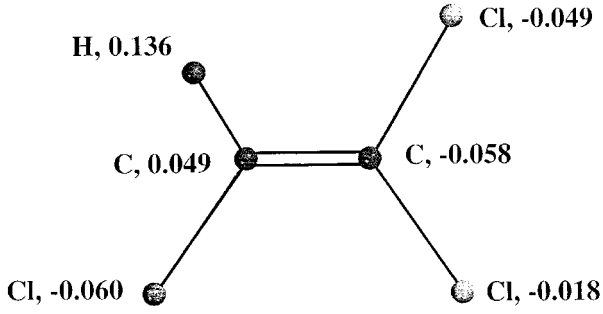

FIGURE 1. MP2 / 6-311 + G(2d, p) CHELPG estimate for the partial atomic charges that best reproduce the molecular electrostatic potential of C_2HCl_3.

cally chosen (based on unit cell dimensions) and an energy accuracy parameter is specified (here, 0.025 kcal/mol). These two values were used to calculate the real-space and reciprocal-space cutoffs necessary to achieve the given accuracy.[19] Short-range van der Waals repulsion energies were computed in the all-image convention, again using the accuracy parameter to determine unit-cell-dependent cutoff radii.[19] Tests of this overall method showed that nonbonded energies were accurate to within 0.05% of their asymptotic values. The method was used for all simulations reported here.

The 1 : 1 clay mineral kaolinite (type 1 : 1 means that each clay layer consists of one sheet of octahedral aluminum oxide bonded to a sheet of tetrahedral silicon oxide) was constructed using experimental coordinates.[20] From this, a supercell [composition $Al_{32}Si_{32}O_{80}(OH)_{64}$] was built (Fig. 2) with a nearly rectangular repeat unit of 20.61 by 17.88 Å in the *ab*-plane. Unlike many other clays, kaolinite does not typically swell along the *c*-axis upon hydration. Nevertheless, we separated the layers for the purpose of simulation: We increased the *c*-axis from 7.4 to 20.0 Å to create a 12-Å interlayer space where the behavior of water and C_2HCl_3 could be modeled. Here kaolinite proves itself to be an interesting model mineral, because it presents two very different types of surfaces to aqueous solution. Artificially expanded pores like those depicted in Figure 2a and b provide the opportunity to use a single simulation to study adsorption to both types of basal external surface that would be found on a kaolinite mineral grain. Slit-pores of

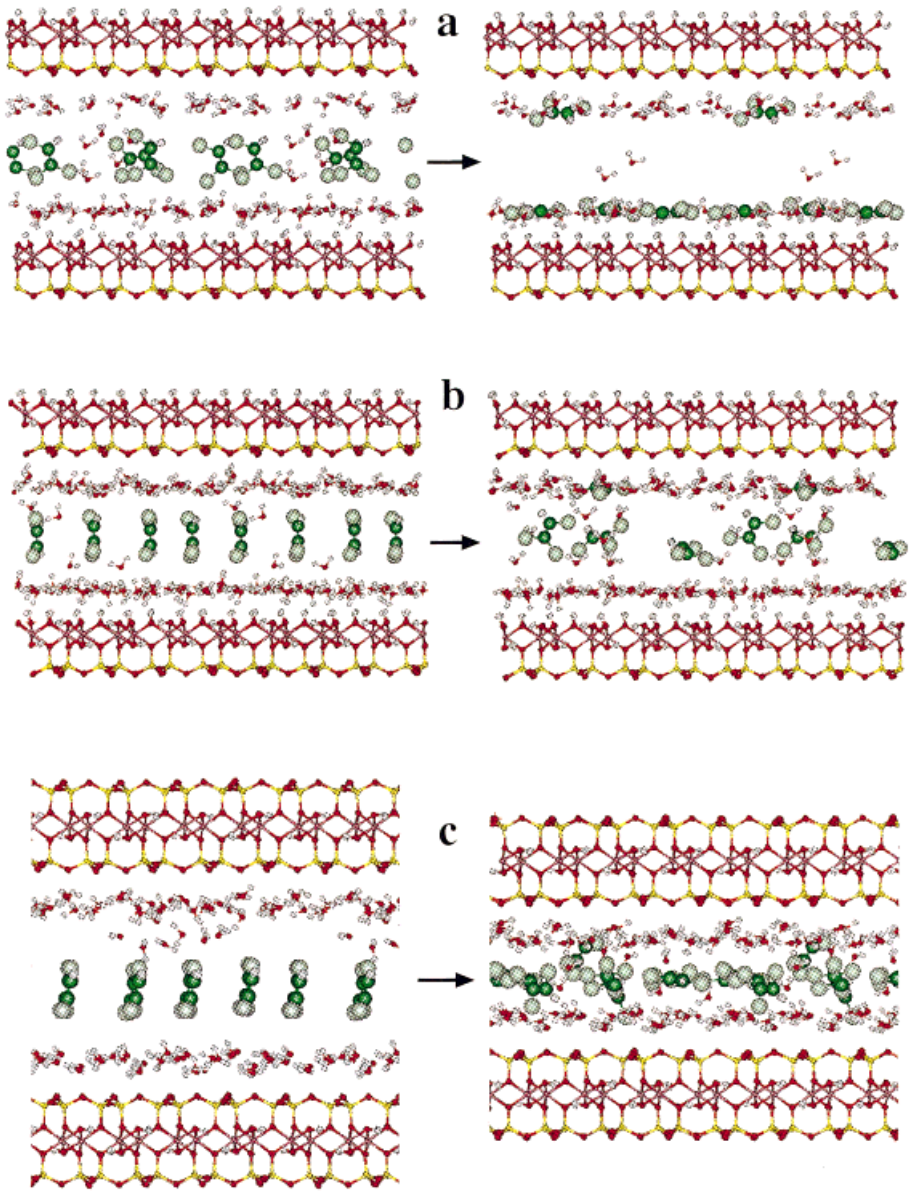

FIGURE 2. Snapshots of initial conditions (left) and typical configurations after molecular dynamics equilibration (right) for C_2HCl_3 added to the interlayer spaces of hydrated clays. The systems are: (a) kaolinite and 0.24 g / g water at constant NVT; (b) kaolinite and 0.39 g / g water at constant NVT; and (c) pyrophyllite and 0.32 g / g water at constant NPT. In this projection of the initial configuration for (c), only four of eight unique C_2HCl_3 molecules are visible.

this type are found in the environment, for example, in kaolinite ''books''[21] and perhaps at interfaces between silicate grains and aluminum oxide coatings.

The kaolinite surfaces were hydrated at two different levels. Either 55 or 89 water molecules were added to the supercell pore, and then distributed on the surfaces during 15-ps molecular dynamics simulations to create hydrated mineral surfaces. On a dry clay basis, these systems contain 24% and 39% water, respectively. Then, four C_2HCl_3 molecules were added to the center of each slit-pore (Fig. 2a and b) and each system was equilibrated for at least 50 ps.

The clay mineral pyrophyllite is the 2 : 1 analog of kaolinite (each layer consisting of an octahedral sheet of aluminum oxide sandwiched between two sheets of silicon oxide), and was also constructed using experimental data.[22] We chose pyrophyllite for preliminary study because it has the same

structure as the smectites, but it is a neutral clay and the interlayer space is thus devoid of the hydrated counterions that would typically be present to complicate simulations. Six unit cells of pyrophyllite were fused to produce an $Al_{24}Si_{48}O_{120}(OH)_{24}$ supercell of neutral, idealized 2 : 1 clay. Again, we expanded the interlayer space and inserted 76 water molecules to give a water content of 32% by weight. We equilibrated the water for 15 ps at constant volume, and then inserted eight C_2HCl_3 molecules into the center of the interlayer space (Fig. 2c). This time, the molecular dynamics were run in the isothermal–isobaric (NPT) ensemble to simulate C_2HCl_3 in a fully hydrated micropore environment with no liquid–gas interfaces.

Because this study is part of a long-term program to investigate organic solvent interactions with environmental surfaces, several simulations were done to test the hydrocarbon and water parameters themselves. An eightfold supercell ($2 \times 2 \times 2$) of solid benzene was constructed by replicating the observed[23] unit cell, resulting in a periodic cell containing 64 benzene molecules. For crystalline octane, the experimental cell[24] was used to construct a $3 \times 3 \times 1$ supercell containing 9 octane molecules. To test the chlorine nonbonded parameters, crystal structures of CCl_4 and C_2Cl_6 were used.[25,26] For CCl_4, the unit cell contains 32 molecules, whereas for C_2Cl_6 a $2 \times 2 \times 3$ supercell was built that contained 48 molecules. All the organic crystals were modeled in the NPT ensemble at simulated temperatures of 100 K.

A box containing 64 C_2HCl_3 molecules was built as a starting point for simulations of liquid C_2HCl_3. The box reached equilibrium after about 150 ps, and data were gathered for a subsequent 50 ps. Finally, a periodic box of 256 water molecules was used to determine the structure and density of the pcff water.

Results and Discussion

Representative snapshots of the three equilibrated C_2HCl_3–water–clay systems are shown in Figure 2. In general, as the loading of water onto the clay surfaces increased, water was more likely to outcompete C_2HCl_3 for clay surface sites, in accord with experimental trends.[27–30] At the lowest water content (Fig. 2a), the kaolin surfaces were not covered by a complete monolayer (Fig. 3a), and all C_2HCl_3 molecules were able to adsorb directly to the clay surface. Approximately 2, 6, 8, and 17 ps of simulation time passed before adsorption of the four unique C_2HCl_3 molecules. Once sorbed, no C_2HCl_3 desorbed from the surface over some 50 ps of subsequent simulation. All adsorbed C_2HCl_3 molecules maintained an orientation that was roughly parallel to the clay basal surface plane. No orientation for adsorbed ethenes has been experimentally demonstrated, but infrared dichroism experiments should be able to probe planar molecules like C_2HCl_3 on oriented clay surfaces.[31]

When the water content of the interlamellar pore was increased to allow full monolayer coverage of the kaolin surfaces, only one of the four C_2HCl_3 molecules was able to sorb directly to the clay surface (Figs. 2b and 3b). This adsorption event happened very early in the simulation, after only 1 ps, so it may have been enabled by kinetic energy imbalances that might model random fluctuations in real systems. Again, the adsorbed C_2HCl_3 did not desorb and its molecular plane remained parallel to the clay surface.

The three C_2HCl_3 molecules that remained at the ''air–water interface'' during this simulation did not adopt any consistent orientation. This may be due to the size of the pore chosen here: The distance between the two water monolayers was about 6 Å, which allowed the C_2HCl_3 molecules to contact both water surfaces simultaneously. Further simulations will investigate larger pores to explore the sorption of C_2HCl_3 to single water surfaces.

A third simulation, of C_2HCl_3 in the interlayer space of hydrated pyrophyllite, modeled even wetter conditions than the previous two. Initially, enough water molecules were present to cover both pyrophyllite surfaces with monolayers, plus six excess waters. After insertion of eight C_2HCl_3 molecules (Fig. 2c), the interlayer space was allowed to collapse under atmospheric pressure. Thus, the entire interlayer region formed a condensed, mixed phase of aqueous C_2HCl_3. The equilibrium d(001) spacing was 18.8 ± 0.1 Å. This is a realistic interlayer spacing for an aquifer clay, because a wide variety of smectites suspended in aqueous solutions of divalent cations exhibit d(001)-spacings of 18.5 to 19.5 Å.[32] In this environment, no C_2HCl_3 molecule was able to sorb parallel to the surface during 50 ps of simulation time. Three C_2HCl_3 molecules were able to insert one Cl atom through the water monolayer to make contact with the clay surface (see Figs. 2c and 3c). Significant bursts of kinetic energy were often added to the interlayer molecules due to oscilla-

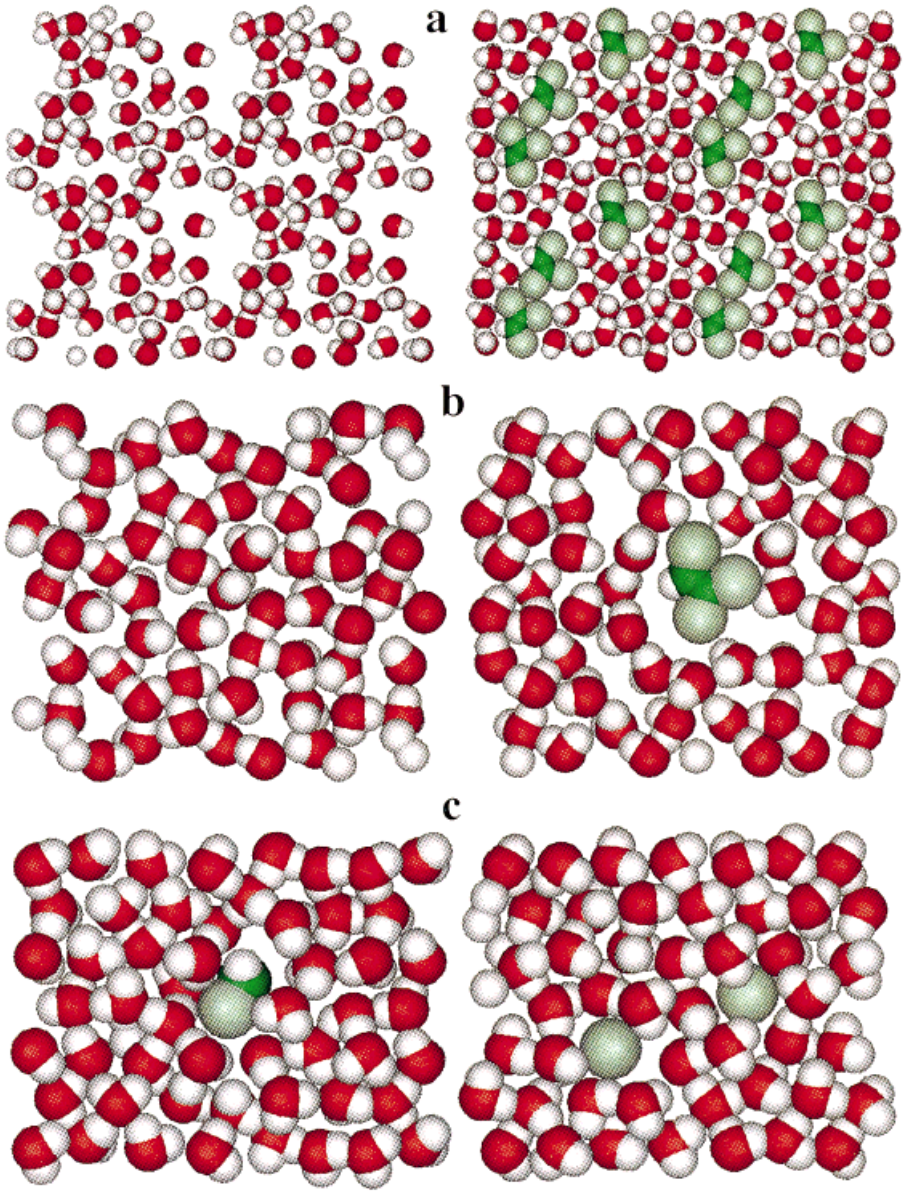

FIGURE 3. Views perpendicular to the clay surfaces of the nearest adsorbed layers for the simulations shown in Figure 2. Part (a) corresponds to the simulation in Figure 2a and shows the layer adsorbed to the alumina surface of kaolinite. The left side shows a snapshot of the initial conditions, whereas a typical configuration after molecular dynamics equilibration is shown on the right. (b) Representative snapshots of the nearest adsorbed layers as seen from the kaolinite siloxane surface during the simulation in Figure 2b. The molecular dynamics began with monolayer water coverage (left) and only one of four C_2HCl_3 was able to displace enough water to adsorb directly to the clay surface (right). (c) Representative snapshots of the nearest adsorbed layers after equilibration as seen from the pyrophyllite siloxane surfaces during the simulation in Figure 2c. At left is the layer adsorbed to the top surface of Figure 2c and at right is the layer adsorbed to the bottom.

tions in the d(001)-spacing (Fig. 4). None of these bursts resulted in the concerted desorption of water that would be required for C_2HCl_3 to sorb parallel to the clay surface, seemingly because of the condensed nature of the interlayer region. Typically, when a sorbed water molecule began to leave the surface under the impetus of some collision, it would quickly collide with other molecules that limited its range of motion and kept it near the surface.

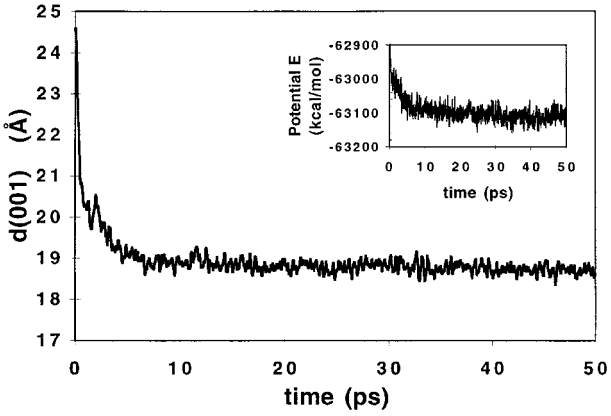

FIGURE 4. Trajectories of the d(001) clay layer spacing and potential energy with time for the simulation in Figure 2c.

The H—C—Cl end of one C_2HCl_3 molecule (at top of interlayer in Fig. 2c) was able to approach the clay surface during the first 5 ps, and remained sorbed nearly perpendicular to the surface for the duration of the simulation. A second C_2HCl_3 molecule pushed one Cl atom of its Cl—C—Cl end toward the surface within the first 10 ps, and held it there until it desorbed after 48 ps had elapsed. A third C_2HCl_3 pushed a Cl atom into the same surface water monolayer (at bottom right of Fig. 2c) from 47 ps until the end of the simulation. Thus, two C_2HCl_3 molecules were always sorbed to the surface, and for a brief time there were three. The other five C_2HCl_3 molecules remained sandwiched between the water monolayers, more or less parallel to the clay surfaces.

These simulations suggest that at least three distinct mechanisms coexist for C_2HCl_3 on clay minerals in the environment. The most stable interaction of C_2HCl_3 with the clay mineral surface is by full molecular contact, coplanar with the clay basal surface. In our simulations, this mechanism was increasingly rare for a more fully hydrated surface, irreversible once it occurred, and preferred more on the hydroxylated alumina-like surface of kaolinite than on the siloxane surface. However, water sorption was also more favored on the alumina surface (i.e., see Fig. 2a), so C_2HCl_3 was only able to outcompete water for the siloxane surface in simulation (Fig. 2b). A second mechanism was adsorption of C_2HCl_3 directly to the surface through single-atom contact between one Cl atom and the surface. This interface was less stable and allowed transient sorption events. Finally, some adsorbed C_2HCl_3 never contacted the clay directly but sorbed onto the first water layer, which was itself adsorbed to the clay surface in a nearly planar configuration.

To test their applicability in solid state simulations, we used the pcff force field parameters to calculate the crystal structures of several representative organic systems, following the procedure by Allinger et al.[33] who used information on isolated molecules as well as on crystal structures to develop force field parameters for hydrocarbons.

The pcff force field modeled the crystal structures and liquid densities of several organic solvents fairly well. Figure 5 displays experimental and simulated crystal structures of benzene, oc-

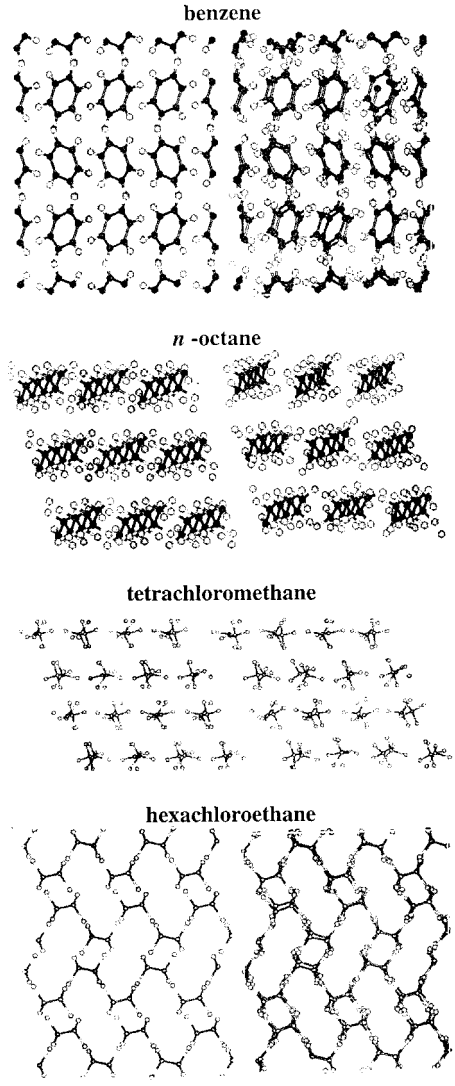

FIGURE 5. Some experimental organic crystal structures (left) and typical snapshots after NPT – molecular dynamics equilibration (right) at 1 bar and 100 K.

tane, CCl_4, and C_2Cl_6, and shows that the basic structures of each are reproduced satisfactorily. The crystal densities of solid benzene and octane, too, were reproduced although the individual unit cell dimensions were obtained less accurately (Table II). The calculated densities of the chlorinated solvents, however, were 3–6% greater than the experimental densities, indicating that either: (a) the charges on Cl atoms should be of greater magnitude; or (b) the balance between repulsion and dispersion on Cl atoms should be shifted to decrease the dispersive forces. Either adjustment should somewhat reduce the attractive forces between dry clay surfaces and C_2HCl_3.

To obtain another estimate for the atomic point charges of Cl, we used Gaussian-94[34] to perform MP2/6-311 + G(2d) geometry optimizations of the Td form of CCl_4 and the D3d form of C_2Cl_6, followed by CHELPG[16–18] optimizations of the point charges that best reproduce the molecular electrostatic potential. The resultant charges were C = −0.372, Cl = +0.093 for CCl_4, and C = −0.406, Cl = +0.135 for C_2Cl_6. In these cases, the charges were opposite in sign to the Mulliken population analyses, which yielded C = +1.18, Cl = −0.30 for CCl_4, and C = +1.30, Cl = −0.43 for C_2Cl_6. Further population analyses using the NBO (natural bond orbital) approach[35] yielded charges of C = −0.310, Cl = +0.077 for CCl_4, and C = −0.259, Cl = +0.086 for C_2Cl_6. Normally, a negative charge was assigned to organic Cl, for example, in CCl_4.[36] We found only two studies where positive charges have previously been assigned to Cl (i.e., in trichloromethane).[37,38] (Both these studies also based their charges on *ab initio* population analyses).

Another approach to defining atomic charges is taken by the ''atoms in molecules'' approach.[39] When the method is applied to C_2HCl_3, negative charges on Cl, slightly larger than those obtained with the CHELPG method, result. In the current analysis we used the CHELPG charges because of our previous success[13] with this procedure. Since electrostatics are such an important contributor to energies in aqueous solution and near mineral surfaces, we intend to further explore charge assignments for chlorohydrocarbons and to refine a new force field in the near future.

For the organic crystal simulations summarized in Table II, the densities after static minimization are about 5% greater than those simulated by molecular dynamics and are always farther from the experimental values. This is an affirmation that, in assessing the validity of parameters for

TABLE II.

Molecular Dynamics (MD) and Minimized Structures (Cell Constants a, b, and c in Ångstrøm, and Angles Between Crystal Axes, α, β, and γ in degrees) of Several Organic Crystals Compared with Experimental Crystal Structures.

Crystal	a	b	c	α	β	γ	ρ (g / cm³)
Benzene							
Experiment[a]	14.88	19.10	13.84	90.0	90.0	90.0	1.055
100 K MD	15.0 ± 0.3	18.6 ± 0.3	14.1 ± 0.2	90 ± 1	90 ± 1	90 ± 1	1.05 ± 0.01
Minimization	14.89	18.35	13.46	90.0	90.0	90.0	1.129
n-Octane							
Experiment[b]	12.66	14.37	11.02	94.7	84.3	105.8	0.891
100 K MD	12.7 ± 0.2	13.6 ± 0.1	11.1 ± 0.1	95 ± 1	85 ± 1	104 ± 1	0.92 ± 0.1
Minimization	12.38	13.27	11.04	95.1	84.8	102.2	0.970
CCl_4							
Experiment[c]	20.18	11.35	19.33	90.0	111.5	90.0	1.940
100 K MD	20.2 ± 0.2	11.0 ± 0.1	19.7 ± 0.2	90 ± 1	114 ± 1	90 ± 1	2.05 ± 0.02
Minimization	19.85	10.74	19.33	90.0	114.8	90.0	2.185
C_2Cl_6							
Experiment[d]	22.56	20.12	19.17	90.0	90.0	90.0	2.169
100 K MD	22.2 ± 0.1	20.1 ± 0.1	18.8 ± 0.1	90 ± 1	90 ± 1	90 ± 1	2.24 ± 0.01
Minimization	21.94	19.92	18.57	90.0	90.0	90.0	2.325

[a] A 2 × 2 × 2 supercell of the structure given in ref. 23.
[b] A 3 × 3 × 1 supercell of the structure given in ref. 24.
[c] Structure given in ref. 25.
[d] A 2 × 2 × 3 supercell of the structure given in ref. 26.

condensed-phase simulations, thermal motion effects need to be included.

At a simulated temperature of 250 K, benzene formed a liquid rather than a solid despite the 279 K melting point of real benzene. One might thereby infer that the nonbonded potentials are somewhat weak in relation to the kinetic energy. The density of the simulated liquid was 0.78 ± 0.02 g/cm^3, more than 10% below the experimental value of 0.877 g/cm^3 at 293 K.[40] The simulated density of liquid C_2HCl_3 at 298 K was also too low, yielding 1.36 ± 0.03 g/cm^3, as opposed to the observed value of 1.464 g/cm^3 at 293 K.[40]

The final parameters that require validation for our ternary clay–water–organic system are those of water itself. Simulations of bulk water yielded a density of 1.08 ± 0.03 g/cm^3. The peaks in the bulk water radial distribution functions were reasonably close to the experimental values,[41] with the H—O peak at 1.84 Å and the first O—O peak at 2.82 Å. Because the simulated density was too large, the simulated O—O peak was necessarily at a shorter distance than the experimental value, which occurred at 2.875 Å.[41]

With regard to interactions between water and clays, enthalpies of water adsorption are known from aqueous immersion calorimetry. These experiments indicate that adsorption of a monolayer of water from the gas phase onto a dry Ca clay, for example, ought to release about 12–15 kcal/mol.[42,43] We used the pcff water model (Table I) to hydrate a Ca-beidellite[13] that was modeled by our clay force field. The calculated hydration energy was only 7 kcal/mol. This indicates that either (a) dispersive attractions between dry clay layers were too strong, or (b) dispersion or electrostatics of water–clay interactions were too weak.

Conclusion

In spite of imperfections that require further research, these studies have shown that molecular dynamics simulations of organic compounds at the clay mineral–solution interface are now possible, yielding meaningful results. Current focus on further parameter development is centered on two problem areas: (a) the development of water parameters suitable for modeling the environment of clay surfaces; and (b) derivation of effective nonbonded potentials for aqueous and sorbed chlorocarbons.

References

1. H. Kerndorff, R. Schleyer, G. Milde, and R. H. Plumb Jr. In *Groundwater Contamination and Analysis at Hazardous Waste Sites*, S. Lesage and R. E. Jackson, Eds., Marcel Dekker, New York, 1992; p. 245.
2. R. Schleyer, H. Kerndorff, and G. Milde, In *Groundwater Contamination and Analysis at Hazardous Waste Sites*, S. Lesage and R. E. Jackson, Eds., Marcel Dekker, New York, 1992, p. 273.
3. Code of Federal Regulations, National Primary Drinking Water Regulations (40 CFR, Part 141), U.S. Government Printing Office, Washington, DC, p. 592.
4. C. C. West, In *Transport and Remediation of Subsurface Contaminants. Colloidal, Interfacial, and Surfactant Phenomena*, D. A. Sabatini and R. C. Knox, Eds., American Chemical Society, Washington, DC, 1992, p. 149.
5. T. J. Estes, R. V. Shah, and V. L. Vilker, *Environ. Sci. Technol.*, **22,** 377 (1988).
6. J. Farrell and M. Reinhard, *Environ. Sci. Technol.*, **28,** 53 (1994).
7. J. Farrell and M. Reinhard, *Environ. Sci. Technol.*, **28,** 63 (1994).
8. G. L. Keldsen, J. B. Nicholas, K. A. Carrado, and R. E. Winans, *J. Phys. Chem.*, **98,** 279 (1994).
9. J. Breu and C. R. A. Catlow, *Inorg. Chem.*, **34,** 4504 (1995).
10. H. Sato, A. Yamagishi, and S. Kato, *J. Phys. Chem.*, **96,** 9377 (1992).
11. H. Sato, A. Yamagishi, and S. Kato, *J. Phys. Chem.*, **96,** 9382 (1992).
12. H. Sato, A. Yamagishi, K. Nata, and S. Kato, *J. Phys. Chem.*, **100,** 1711 (1996).
13. B. J. Teppen, K. Rasmussen, P. M. Bertsch, D. M. Miller, and L. Schäfer, *J. Phys. Chem. B*, **101,** 1579 (1997).
14. *MSI, Insight II User Guide, Version* 4.0.0, Molecular Simulations, Inc., San Diego, CA, 1996.
15. *MSI, Discover User Guide, Versions* 2.9.8, 96.0, *and* 4.0.0, Molecular Simulations, Inc., San Diego, CA, 1996.
16. L. E. Chirlian and M. M. Francl, *J. Comput. Chem.*, **8,** 894 (1987).
17. C. M. Breneman and K. B. Wiberg, *J. Comput. Chem.*, **11,** 361 (1990).
18. M. M. Francl, C. Carey, L. E. Chirlian, and D. M. Gange, *J. Comput. Chem.*, **17,** 367 (1996).
19. N. Karasawa and W. A. Goddard III, *J. Phys. Chem.*, **93,** 7320 (1989).
20. D. L. Bish, *Clays Clay Miner.*, **41,** 738 (1993).
21. J. B. Dixon, In *Minerals in Soil Environments*, 2*nd Ed.* (Soil Science Society of America Book Series 1), J. B. Dixon and S. B. Weed, Eds., Soil Science Society of America, Madison, WI, 1989, p. 467.
22. J. H. Lee and S. Guggenheim, *Am. Mineral.*, **66,** 350 (1981).
23. K. D. Gibson and H. A. Scheraga, *J. Phys. Chem.*, **99,** 3765 (1995).
24. H. Mathisen, N. Norman, and B. F. Pedersen, *Acta Chem. Scand.*, **21,** 127 (1967).

25. S. Cohen, R. Powers, and R. Rudman, *Acta Cryst*., **B35,** 1670 (1979).
26. D. Hohlwein, W. Nägele, and W. Prandl, *Acta Cryst*., **B35,** 2975 (1979).
27. W. F. Spencer, W. J. Farmer, and W. A. Jury, *Environ. Toxicol. Chem*., **1,** 17 (1982).
28. C. T. Chiou and T. D. Shoup, *Environ. Sci. Technol*., **19,** 1196 (1985).
29. K.-U. Goss, *Environ. Sci. Technol*., **26,** 2287 (1992).
30. K.-U. Goss and S. J. Eisenreich, *Environ. Sci. Technol*., **30,** 2135 (1996).
31. W. P. Gates, B. J. Teppen, and P. M. Bertsch, *Schriftenr. Angew. Geowiss*., **1,** 41 (1997).
32. D. M. C. MacEwan and M. J. Wilson, In *Crystal Structures of Clay Minerals and Their X-Ray Identification*, G. W. Brindley and G. Brown, Eds., Mineralogical Society, London, 1980, p. 197.
33. N. L. Allinger, Y. H. Yuh, and J.-H. Lii, *J. Am. Chem. Soc*., **111,** 8551 (1989).
34. M. J. Frisch, G. W. Trucks, H. B. Schlegel, P. M. W. Gill, B. G. Johnson, M. A. Robb, J. R. Cheeseman, T. A. Keith, G. A. Petersson, J. A. Montgomery, K. Raghavachari, M. A. Al-Laham, V. G. Zakrzewski, J. V. Ortiz, J. B. Foresman, J. Cioslowski, B. B. Stefanov, A. Nanayakkara, M. Challacombe, C. Y. Peng, P. Y. Ayala, W. Chen, M. W. Wong, J. L. Andres, E. Replogle, R. Gomperts, R. L. Martin, D. J. Fox, J. S. Binkley, D. J. Defrees, J. Baker, J. P. Stewart, M. Head-Gordon, C. Gonzalez, and J. A. Pople, *Gaussian-94, Rev. B.3*, Gaussian, Inc., Pittsburgh, PA, 1995.
35. A. E. Reed, L. A. Curtiss, and F. Weinhold, *Chem. Rev*., **88,** 899 (1988).
36. F. J. Luque, M. Bachs, C. Alemán, and M. Orozco, *J. Comput. Chem*., **17,** 806 (1996).
37. T. Fox, B. E. Thomas, M. McCarrick IV, and P. A. Kollman, *J. Phys. Chem*., **100,** 10779 (1996).
38. H. J. Böhm and R. Ahlrichs, *Mol. Phys*., **54,** 1261 (1985).
39. R. W. F. Bader, *Atoms in Molecules: A Quantum Theory*, Oxford University Press, New York, 1990, p. 438.
40. D. R. Lide, Ed., *CRC Handbook of Chemistry and Physics, 73rd Ed*., CRC Press, Boca Raton, FL, 1992.
41. A. K. Soper and M. G. Phillips, *Chem. Phys*., **107,** 47 (1986).
42. R. Keren and I. Shainberg, *Clays Clay Miner*., **28,** 204 (1980).
43. M. H. Fu, Z. Z. Zhang, and P. F. Low, *Clays Clay Miner*., **38,** 485 (1990).